POWER EVALUATION FOR FLUTTER-BASED ELCTROMAGNETIC ENERGY HARVESTER USING CFD SIMULATIONS

J. Park [1], G. Morgenthal [2], S. Kwon[3] and K. H. Law[1]
[1] Department of Civil and Environmental Engineering,
Stanford University, Stanford, CA, USA
[2] Institute for Structural Engineering,
Bauhaus University, Weimar, Germany
[3] KOCED Wind Tunnel Center, Department of Civil Engineering
Chonbuk National University, Chonju, Korea

ABSTRACT

Structural instability caused by self exciting aerodynamic forces (flutter) can be used as an effective input source for small scale energy harvesters. The self exciting aerodynamic force exerted on a T-shape cantilever causes periodic vibration, which can be converted into electric power through an electromagnetic transducer. Due to the complexities inherent in the fluid-structure interaction between the cantilever harvester and wind flow, analyzing the structural response of the cantilever and estimating the power output from the flutter based energy harvester are challenging. VXflow, a CFD code based on the vortex particle method, is employed in this study to simulate the wind induced responses of a T-shape cantilever beam and to estimate the power output extracted from the flutter vibration. The estimated aerodynamic damping parameter, together with the mechanical and electromagnetic damping parameters, in the harvester are then used to find the flutter critical wind speed where flutter starts and the proper load resistance.

KEYWORDS

Flutter, CFD simulation, aerodynamic instability, energy harvesting, electromagnetic.

INTRODUCTION

Energy harvesting has been an active research area as demands for renewable energy sources increase. Energy harvesting systems refer to devices that capture and transform energy from the environment into electricity. Unlike conventional, large-scale renewable energy generating systems such as wind turbines, thermal generators, and solar panels, energy harvesting devices mostly target on powering small electronic devices. For example, many researchers are investigating how to supply power to wireless sensor modules using energy harvesters (Roundy and Wright 2004). If such sensors can be operated solely on power generated from an energy harvester, the need for regularly changing batteries can be eliminated and the maintenance cost of wireless sensor network can thus be reduced.

Wind energy has long been used to generate power mostly using wind turbines by exploiting the blades' lift and drag forces to rotate an electromagnetic generator. This conventional approach for generating power is, however, difficult to apply to small scale energy harvesters, because small size generators are difficult to make and have low efficiency. Wind induced vibrations have been suggested as an alternate input source for small scale energy harvesters. Wind induced vibrations have been used to mechanically strain piezoelectric transducers to generate power (Allen and Smits 2001; Sun *et al.* 2011) and to generate inductance power in electromagnetic transducers (Jung *et al.* 2011). Aero-elastic instability phenomenon, which is referred to as flutter, has also been suggested as an input source for energy harvesters because of its potential capability for generating electrical power. Flutter induced vibration of T-shape cantilever beam and plate have been used to mechanically strain piezoelectric patches to generate power (. Kwon 2010; Bryant *et al.* 2011). A leaf-like structure has also been proposed to convert cross-flow flutter into electricity using Poly Vinylidene Fluoride (Li *et al.*2011).

Flutter is a phenomenon that engineers have strived to prevent since flutters on air plane wings and bridge girders can lead to destructive structural failures. In bridge engineering, particularly, researchers have conducted myriad wind tunnel tests to understand flutter phenomenon using scaled structural models. With advancements in computing power, computational fluid dynamics (CFD) has also been used and played important roles in

designing aerodynamically stable bridge sections (Larsen 1998). In this paper, on the contrary, we seek to design aerodynamically unstable shapes to invoke the flutter induced vibration and to use it as an input source for the electromagnetic energy harvester. We employ VXflow, a CFD code based on Vortex particle method (Morgenthal 2007), to analyze the vibrational responses and the power output from the energy harvester under different wind speeds and electrical load resistances.

THEORETICAL BACKGROUNDS

Electromagnetic (EM) transducer

Electromagnetic based energy harvesters can be built using an inertial frame configuration, in which the relative movement between the magnets and the coils are induced by the vibration of the inertial frame. The vibration system can be described as a forced vibration equation as follows (Beeby 2007):

$$m\ddot{z}(t) + c_t\dot{z}(t) + kz(t) = -m\ddot{y}(t) \tag{1}$$

where m, c_t and k are, respectively, the mass, total damping and stiffness of the vibration frame; y and z represent the inertial frame displacement and the relative displacement between the magnet and the coil, respectively. The total damping coefficient c_t includes both the mechanical damping and the electrical damping $(c_t = c_m + c_e)$. The mechanical damping c_m $(c_m = 2m\zeta_m\omega_n)$ is expressed in terms of damping ratio ζ_m and the natural frequency ω_n, and the electrical damping c_e is expressed as (El-hami *et al.* 2001):

$$c_e = \frac{(Nl\beta)^2}{R_L + R_C + j\omega L_C} \tag{2}$$

where N, l and β are, respectively, the number of coil turns, the coil length exposed to the magnetic flux and the average flux density. Furthermore, R_L, R_C and L_C are, respectively, the load resistance, the coil resistance and the coil inductance, and ω is the angular frequency in the motion between the magnet and the coil. The generated energy is equivalent to the energy extracted by the electrical damping from the system as:

$$P = c_e\dot{z}^2 \tag{3}$$

where $\dot{z}$ is the relative speed between the magnet and the coil. Note that $\dot{z}$ is itself a function of electrical damping c_e since the total damping c_t includes c_e to suppress the displacement z. That is, power generation depends on both the electrical and structural parameters.

Analytic descriptions for flutter

In wind engineering, the motion of a bridge girder responding to the self excited forces by wind is described by the equations corresponding to bending and torsional modes as (Morgenthal 2002):

$$m\ddot{h} + 2m\zeta_h\omega_h\dot{h} + m\omega_h^2 h = F_L(t) \tag{4}$$

$$I\ddot{\alpha} + 2I\zeta_\alpha\omega_\alpha\dot{\alpha} + I\omega_\alpha^2\alpha = F_M(t) \tag{5}$$

where m and I are, respectively, the mass and the moment of inertia, ζ_h and ζ_α are, respectively, the damping ratios in bending and torsional modes, h and α are, respectively, the deflection and the rotation, ω_h and ω_α are, respectively, the natural circular frequencies for the bending and torsional modes. The aerodynamic force $F_L(t)$ and aerodynamic moment $F_M(t)$ are given as (Larsen 1997):

$$F_L(t) = \frac{1}{2}\rho U_\infty^2 B\left[KH_1^*(K)\frac{\dot{h}}{U_\infty} + KH_2^*(K)\frac{B\dot{\alpha}}{U_\infty} + K^2H_3^*(K)\alpha + K^2H_4^*(K)\frac{h}{B}\right] \tag{6}$$

$$F_M(t) = \frac{1}{2}\rho U_\infty^2 B^2\left[KA_1^*(K)\frac{\dot{h}}{U_\infty} + KA_2^*(K)\frac{B\dot{\alpha}}{U_\infty} + K^2A_3^*(K)\alpha + K^2A_4^*(K)\frac{h}{B}\right] \tag{7}$$

where ρ , U_∞ and B are, respectively, the air density, the free stream wind speed and the section length. H_1^* , H_2^* , H_3^* and H_4^* are the flutter derivatives in the bending mode, and A_1^* , A_2^* , A_3^* and A_4^* are the flutter derivatives in the torsional mode. Furthermore, K is the non-dimensional reduced frequency defined as:

$$K = \frac{\omega B}{U_\infty} \tag{8}$$

The self exciting forces are dependent on the deflection and the rotation of the section and these forces are strongly affected by the section shape. Substituting Eq. 7 into Eq. 5 and neglecting the bending mode lead to the following second order differential equation representing a simple 1-DOF, free vibration problem:

$$I\ddot{\alpha} + \left\{2I\zeta_\alpha\omega_\alpha - \frac{1}{2}\rho U_\infty B^3 K A_2^*(K)\right\}\dot{\alpha} + \left\{I\omega_\alpha^2 - \frac{1}{2}\rho U_\infty^2 B^2 K^2 A_3^*(K)\right\}\alpha = 0 \tag{9}$$

The terms $2I\zeta_\alpha\omega_\alpha$ and $1/2\rho U_\infty B^3 K A_2^*(K)$ are, respectively, the mechanical and the aerodynamic damping in torsional mode. The system damping and stiffness are affected by the flutter derivatives whose values are highly depending on the geometry of the cantilever section and the wind speed. The analytical flutter derivatives for the oscillating thin plates have been derived by Scanlan and Tomko (1971). In general, however, the flutter derivatives of a section whose geometry deviates from a simple thin plate are difficult to estimate analytically. Wind tunnel tests or CFD simulations are used to find the flutter derivatives for sections with complex geometry.

Aerodynamic instability analysis based on CFD

Computational fluid dynamics (CFD) has been employed to evaluate the aerodynamic instability of bridge sections. For example, the computer code DVMFLOW was used for evaluating aerodynamic stability of different bridge sections (Larsen and Walther 1998). VXflow, the CFD code employed in this study, has been used to compare the critical wind speed and frequency for various bridge sections studied in the literature (Morgenthal 2002). The instability is conventionally evaluated based on the flutter derivatives, which are closely related to the system damping. The flutter derivatives can be estimated by forced vibration simulation. Assuming that the periodic deflection and rotation with frequency ω cause the motion induced forces with the same frequency ω but with phase shift angle φ , Eqs. 4 and 5 can be combined with the forcing terms (Eqs. 6 and 7) and rearranged as follows (Larsen and Walther 1998):

$$C_L e^{i(\omega t-\varphi)} = 2K^2\left[(iH_1^* + H_4^*)\frac{h}{B} + (iH_2^* + H_3^*)\alpha\right]e^{i\omega t} \tag{10}$$

$$C_M e^{i(\omega t-\varphi)} = 2K^2\left[(iA_1^* + A_4^*)\frac{h}{B} + (iA_2^* + A_3^*)\alpha\right]e^{i\omega t} \tag{11}$$

where C_L and C_M are, respectively, the lift and moment coefficients representing the ratios of the lift force and moment to the wind flow force acting on the section. The flutter derivatives can be found based on the measured amplitude of the coefficients C_L and C_M and the phase difference φ between the imposed periodic motion and the force coefficients as in Eqs. 10 and 11. Inserting the force terms (Eqs. 6 and 7) expressed in terms of the flutter derivatives into the motion equations (Eqs. 4 and 5) leads to a system dynamic equation.

The eigenvalues of the derived system dynamic equation depict the characteristics of structural responses corresponding to wind induced forces. That is, when the real part of the complex eigenvalues of the system is negative, the system becomes unstable with excessive vibrational responses (Morgenthal 2000). In this paper, we only consider the torsional mode of the T-shape cantilever energy harvester by treating the cantilever beam as a rigid body (1-DOF in rotation). In this case, the stability of the cantilever section can be evaluated by only considering the sign of the coefficient $\dot{\alpha}$ (angular velocity) in Eq. 9, which represents the system damping term. The negative system damping would indicate inputting energy into the system, which leads to exponentially increasing responses.

FLUTTER SIMULATION USING VXflow

The flutter critical wind speed, where the flutter starts, the oscillating frequency and the maximum tip displacement of the cantilever in the flutter based energy harvester are essential information for estimating the power output from the harvester. Due to the complexities inherent in the fluid structure interactions, it is almost impossible to analytically estimate this information. In this study, we use VXflow to simulate the vibrational responses of the T-shape cantilever in the flutter based energy harvester. In addition, the flutter derivatives at different wind speeds are estimated to find the flutter critical wind speed. For the VXflow simulation, we only considered the structural intrinsic damping. The influences of the electromagnetic transducer, which imposes an additional electrical damping to the system, on the responses will be considered at the later part of this paper.

Descriptions for the energy harvester model

The configurations, structural and electrical parameters for the flutter based energy harvester are depicted in Figure 1. The T-shape cantilever is used to induce the large vortex induced force and, therefore, to initiate flutter at low wind speed. The magnets are attached to the tip of the cantilever, whose interaction with the coils induces the inductive voltage in the energy harvester. The coils are attached to the inertial frame. VXflow supports 2-D section analysis and assumes the section is rigid. Therefore, it is necessary to approximate the deflection of the cantilever in terms of the rotational motion of an equivalent rigid bar. To this end, the spring-supported rigid body is derived by seeking the equivalent rotational stiffness, rotational mass and reduced length as shown in Figure 1.

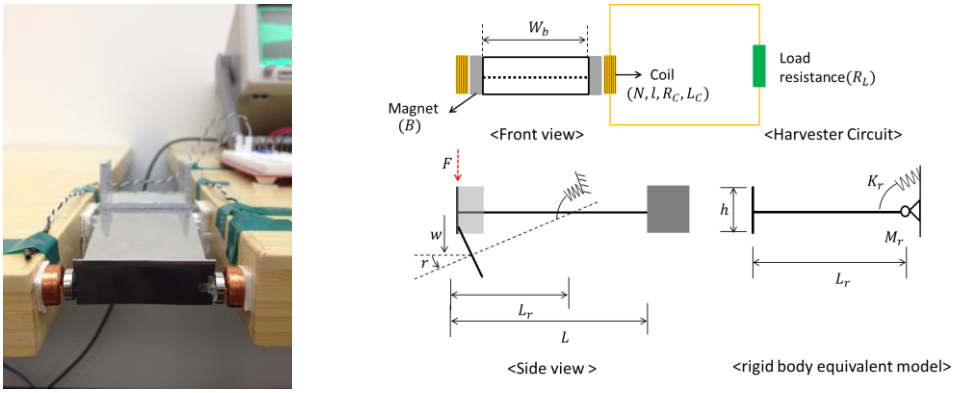

Figure 1: Energy harvester model and the equivalent rigid body model

The vertical deflection and the rotation under a unit force F exerting on the cantilever tip are calculated, respectively, as $w = FL^3/3EI$ and $r = FL^2/2EI$. The length L_r of the rigid body section with the same rotation r can be approximated using the linear relationship $L_r r = w$, which results in $L_r = 2/3L$, where L is the length of the cantilever beam. The corresponding rotational stiffness is then given as $K_r = FL_r/r = 4EI/3L$. Furthermore, the rotational mass (the moment of inertia) is computed as $M_r = mL_r^2 = 4mL^2/9$. The parameters for the original cantilever, the equivalent rigid frame and the electromagnetic transducer are summarized in Table 1.

Table 1: Parameters for the energy harvester

Model dimensions	Rotational mode	Electromagnetic parameters
W_b (width) = 0.05 m	L_r (reduced length) = 0.0533 m	R_C (Coil resistance) = 220 Ω
L (length) = 0.08 m	M_r (rotational mass) = $2.62 \cdot 10^{-4}$ Kg	N (Coil turns) = 2800
h (tip height) = 0.02 m	K_r (torsional stiffness) = 0.262 Nm	β (Magnetic flux density)
t (thickness) = $1.016 \cdot 10^{-4}$ m	ω_r (rotational frequency) = 31.7 rad/sec	l (height of magnet) = 0.01 m
m (mass) = 0.0046 Kg		
E (Elastic modulus) = 180GPa		
I (moment of inertia) = $4.37 \cdot 10^{-15}$ m^4		
K (stiffness) = 4.6089 N/m		
ω (natural frequency) = 31.7 rad/sec		
ζ_m (damping ratio) = 0.0085		

Forced vibration

The change in sign of A_2^* derivative can be used to identify the stability of the section and torsional flutter of the SDOF system (Larsen and Walther 1998). We estimate the A_2^* flutter derivative using the forced vibration mode in VXflow at different wind speeds. The results are summarized in Figure 2. The A_2^* flutter derivative generally increases with the free stream wind speed, meaning that the system becomes increasingly unstable at higher wind speed. For the cantilever energy harvester model described in Table 1, the A_2^* flutter derivative transits from the negative value into the positive value around U_∞= 3.6 ~ 3.7 m/s, which represents the flutter critical wind speed separating the stable and unstable regions of the system response.

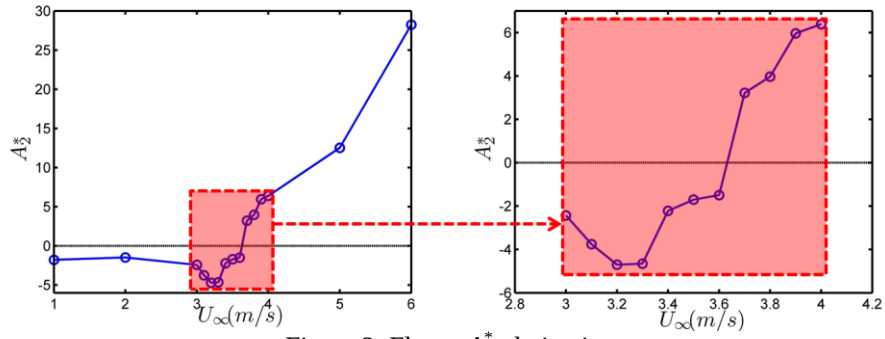

Figure 2: Flutter A^*_2 derivatives

Fluid structure interaction analysis using VXflow

The responses of the flutter based energy harvester are simulated by the fluid structure interaction mode in VXflow. Figure 3 shows a snap-shot of the T-shape cantilever vibration showing the equivalent rigid frame model. Figure 4 shows the cantilever tip displacement time series corresponding to the wind speeds for 3 m/s and 4 m/s, respectively, which are lower and higher than the critical wind speed (3.6 ~ 3.7 m/s) leading to the onset of the flutter. As shown in Figure 4b, when the wind speed is above the flutter critical wind speed, the amplitude of the tip displacement increases until reaching its maximum and is maintained then in an almost constant level, whose responses resembles periodic forced vibration. The exponentially growing trend in the displacement is due to the negative damping in the system induced by the self exciting aerodynamic forces. After reaching its maximum amplitude, the oscillation is bounded due to the nonlinear effects at the very large oscillation amplitudes and the geometric constraints

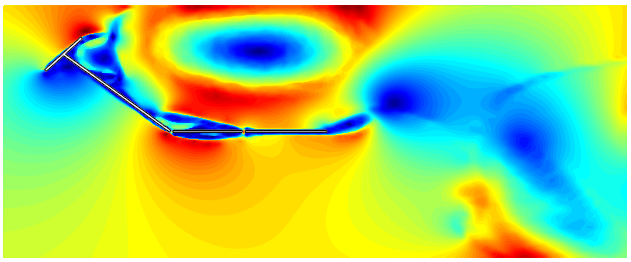

Figure 3: Fluid-structure interaction simulation

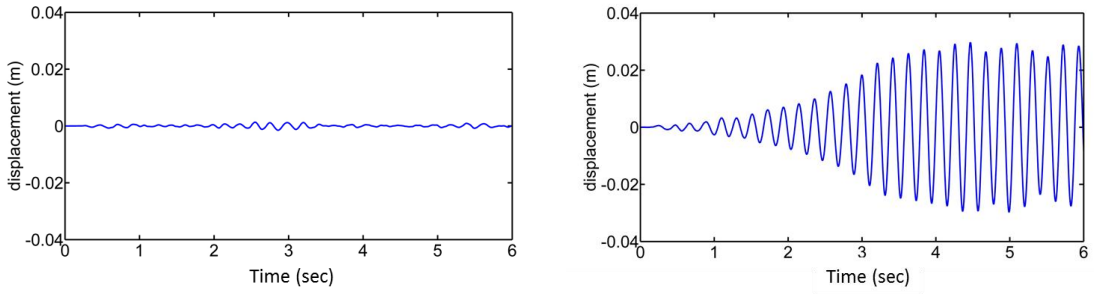

(a) U = 3 m/s (Stable) (b) U = 4 m/s (Unstable)

Figure 4: Tip displacement of the cantilever corresponding to different wind speeds

EXPERIMENT RESULTS

The flutter based energy harvester includes three damping mechanisms: mechanical damping, electrical damping and aerodynamic damping. The mechanical damping dissipates mechanical energy of the cantilever, and the electrical damping extracts energy from the system and converts it into electrical energy. The aerodynamic damping either extracts energy from the system or inputs energy into the system depending on the wind speed (energy is infused into the system when the wind speed exceeds the flutter critical speed). The three damping mechanisms determine the vibrational motion of the flutter based energy harvester. In particular, the structural stability of the cantilever is determined by the relative magnitudes among the three damping coefficients. This section describes how to estimate the flutter critical wind speed based on the relationship among the three damping parameters. We then describe the characteristics of the power output and the method for selecting the optimum load resistance in the energy harvester for a given wind speed.

Prediction of flutter speed based on three damping coefficient

Free vibration tests have been conducted to estimate the damping ratios (i.e., mechanical and electrical damping) of the energy harvester, which are then converted into the mechanical damping and electrical damping coefficients. Figure 5 shows the voltage time series generated by the free vibration tests with different electrical resistances. This figure clearly shows that the decaying rate of the amplitude peaks decreases with load resistance. The amplitude decaying rate of peaks enables us to estimate the total damping ratio. The difference between the total damping and the mechanical damping then gives the electrical damping. Figure 6 shows the voltage time series generated from the vibration caused by wind flow with different wind speeds. The voltages are measured using the NI-USB 6009 DAQ driver, whose internal resistance is 144 $K\Omega$ (R_L = 144 $K\Omega$). Note that when R_L = 144 $K\Omega$, the total damping ($c_t = c_m + c_e$) is almost equal to the structural intrinsic damping since the electric damping asymptotically converges to zero as R_L approaches infinity (essentially open circuit). We can observe that the voltage amplitude increases with free stream wind speed. Based on the exponentially increasing trend in the voltage amplitude, we can infer that the energy is being inputted to the system (negative system damping). In addition, comparing the increasing rates of the amplitude, we can conclude that the aerodynamic damping decreases with wind speed.

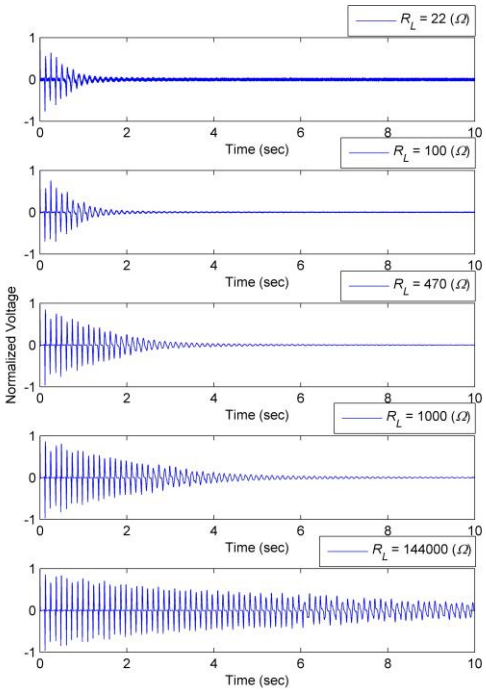

Figure 5: Free vibration

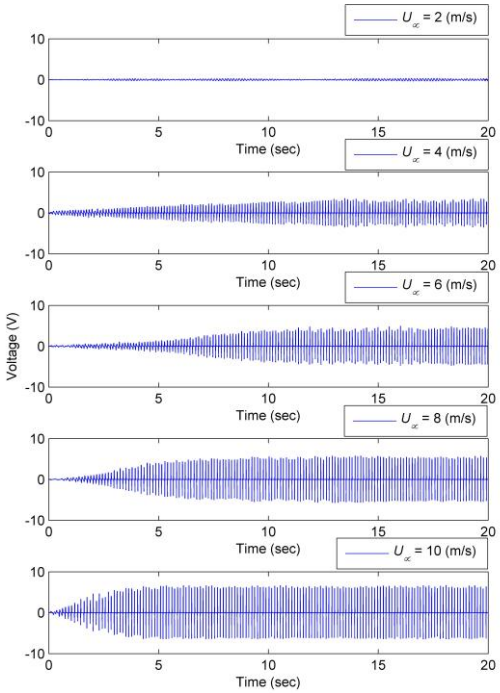

Figure 6: Wind induced vibration (R_L=144,000Ω)

By changing the load resistance (from 22 Ω to 144000Ω), the electric damping coefficient c_e are estimated, from which the empirical models for c_e (Eq. 2) can be fitted. Note that the term $N\beta l$ in Eq. 2 can be found by measuring each of the terms N, β and l. Measuring β, however, requires complicated magnetic flux analysis. The electrical damping coefficients follow the trend represented in the empirical model for c_e. It is worth noting that the electrical damping coefficient is 6~7 times larger than the mechanical damping coefficient when the load resistance is low (ζ_e = 5~6 %, ζ_m = 0.85 %). The measurements and the empirical models for the electrical

damping coefficients are summarized as shown in Figure 7. The aerodynamic damping coefficients are estimated from the A_2^* flutter derivative obtained by the VXflow forced simulations for different wind speeds. The aerodynamic damping coefficient c_a is defined as $1/2\,\rho U_\infty B^3 K A_2^*(K)$ in this paper; therefore the system damping including the additional electrical damping c_e in Eq. 9 is given as $c_m + c_e - c_a$ (note that the actual aerodynamic damping is $-c_a$).

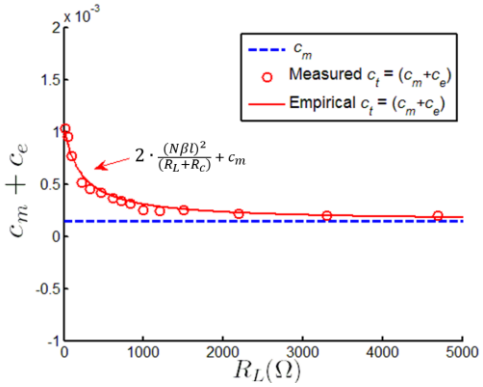

Figure 7: Total damping coefficient

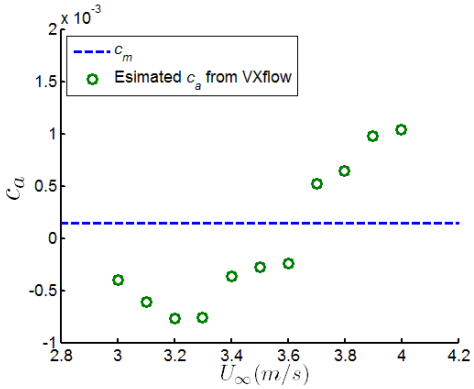

Figure 8: Estimated aerodynamic damping coefficient

Based on Eq. 9, when the aerodynamic damping coefficient c_a exceeds the sum of the electrical and mechanical dampings (i.e., $c_m + c_e \leq c_a$), flutter starts and the system becomes unstable. Since the mechanical damping coefficient is constant and the electrical damping coefficient is a function of load resistance, the sum of mechanical and electrical damping decreases with load resistance as shown in Figure 7. The aerodynamic damping coefficient c_a generally increases with free stream wind speed as shown in Figure 8 (actual aerodynamic damping effect decreases with wind speed). Therefore, the system damping ($c_m + c_e - c_a$) decreases with the wind speed and transits into negative value above a certain wind speed. In this sense, the flutter critical wind speed can be assumed to be the wind speed where the sum of mechanical and electrical damping coefficients and the aerodynamic damping coefficient are equal. When the electromagnetic transducer is open ($R_L = \infty$), the total damping c_t is equal to the structural damping. As shown in Figure 8, the aerodynamic damping coefficient c_a exceeds this structural damping (shown as dashed line) at the wind speed between 3 m/s and 4 m/s; both the experimental tests and the VXflow simulations show that flutter starts at the estimated wind speed range. If the electromagnetic transducer is connected ($R_L < \infty$), the flutter critical speed increases due to the increased total damping c_t.

Amount of available fluid energy

To investigate the influences of electrical damping on the flutter critical speed and the power output, the displacement and the root mean square (RMS) power are measured experimentally with the wind speed of 4 m/s, which are summarized in Figures 9 and 10, respectively. Based on the displacement and the power measurement, we can assume that flutter starts at the load resistance about 1200 ~1500 Ω. Note that the comparison of damping coefficients (Figures 7 and 8) would predict that the flutter starts at much lower resistance. There are two possible reasons for the deviation: i) to induce the initial relative motion between the coil and the magnet, more excessive input energy rate might be needed to initially overcome the static condition of the coil and the magnet, and ii) the experimental model is a flexible cantilever instead of a rigid frame as a assumed using VXflow for estimating the aerodynamic damping coefficients.

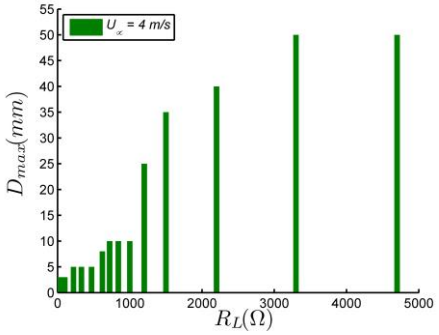

Figure 9: Maximum displacement (U_∞ = 4 m/s)

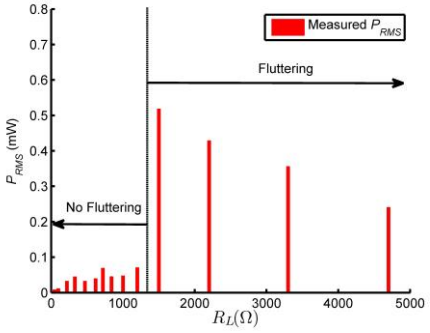

Figure 10: RMS power (U_∞ = 4 m/s)

As shown in Figure 9, the maximum cantilever tip displacement starts to increase when the load resistance reaches about 680 Ω and abruptly jumps at R_L = 1200 Ω. The maximum displacement of 55 mm measured from the experiment is larger than 40 mm estimated from VXflow (Figure 4b), probably because the physical cantilever model experiences large flexural deformation that is not captured by VXflow's rigid body modeling. The electromagnetic transducer starts to generate power from the point where the cantilever starts to vibrate with large displacement as shown in Figure 10. Note that the generated power is not directly proportional to the displacement because the power is also a function of the electrical damping coefficient c_e which decreases with the load resistance.

The available energy from the flutter based energy harvester depends on the wind speed. Furthermore, the extracted energy is determined by the load resistance R_L. The influences of the wind speed and the load resistance on the RMS voltage and the RMS power are summarized in Figures 11 and 12, respectively. In general, it can be observed that the level of the RMS voltage and the RMS power increase with the wind speeds. The voltage and the power curves are discontinuous in that only above a certain load resistance does energy harvester produce energy and this starting load resistance is affected by the wind speed. Note that when wind speed is 10 m/s, the power curve is continuous over all the load resistance range meaning that the flutter always occurs regardless of the R_L. Furthermore, in this case, the maximum power occurs when R_L = R_C as in the inertial frame based electromagnetic harvester case. In other cases, the optimum load resistance should be carefully chosen considering the starting point of the flutter.

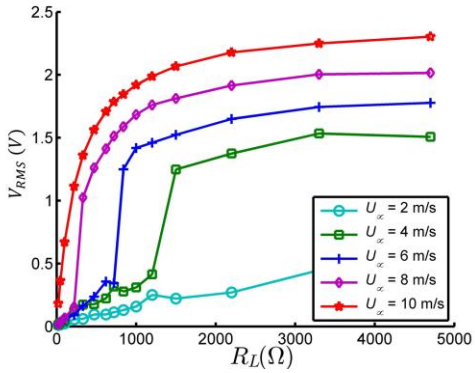

Figure 11 RMS voltage for different wind speeds

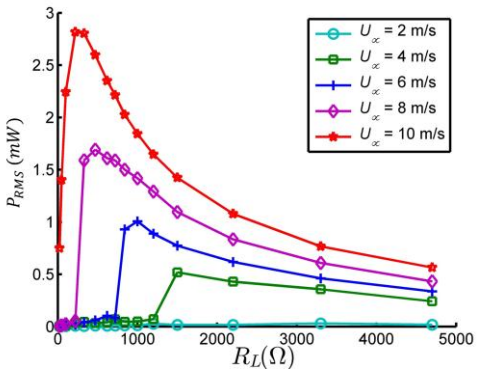

Figure 12 RMS power for different wind speeds

CONCLUSIONS

This paper describes how a CFD simulator VXflow can be used to estimate the flutter critical wind speed and the power output of the flutter based electromagnetic energy harvester. The aerodynamic damping effect is estimated from the flutter derivatives obtained from VXflow forced vibration simulations. Flutter seems to start when the negative aerodynamic damping coefficient exceeds the sum of structural and electrical damping. Below the critical wind speed the fluid extracts energy from the system and above it feeds energy into the system. This analysis gives us the insight how to determine the load resistance, which is one of the most important parameters, by examining the two basic conditions: i) the initiation of the flutter and ii) generation of electrical power. The rigid body model in VXflow appears to approximate the cantilever flutter speed well, but is not sufficient to accurately estimate the large displacement of the cantilever. The cantilever model used in the experiment is very flexible, which may have led to the differences in the comparison of the damping coefficients comparison. If a stiffer cantilever model is used, the deviation in the results from VXflow simulation and the experiment might be reduced. Nevertheless, CFD simulations could be used to optimise the geometry of the wind induced energy harvester. In future work, the CFD model can be extended to take into consideration beam bending in order to estimate the responses more accurately.

ACKNOWLEDGMENTS

This research is partially supported by the US National Science Foundation under Grant No. CMMI-0824977. The third author gratefully acknowledges the support of oversea research fund by Chonbuk National University. Any opinions, findings, and conclusions or recommendations expressed in this paper are those of the authors and do not necessarily reflect the views of the National Science Foundation.

REFERENCES

Allen, J.J. and Smits, A.J. (2001), "Energy harvesting eel," *Journal of Fluids and Structures*, 15, 629–640.

Beeby, S.P., Torsh, R.N., Tudor, M.J., Glynne-Jones, P., O'Donnell, T., Saha, C.R. and Roy, S. (2007), "Amirco electromagnetic generator for vibration enrgy harvesting," *Journal of Micromechanics and Microengineering*, 17, 1257-1265.

Bryant, M., Wolff, E. and Garcia E. (2011), "Aeroelastic flutter energy harvester design: the sensitivity of the driving instability to system parameters," *Smart Materials and Structures*, 20, doi:10.1088/0964-1726/20/12/125017

El-hami, M., Glynne-Jones, P., White, N.M., Hill, M., Beeby, S., James, E., Brown, A.D. and Ross, J.N. (2001), "Design and fabrication of a new vibration-based electromechanical power generator," *Sensors and Actuators A: Physical*, 92, 335–342.

Jung, H., Kim, I. and Jang, S. (2011), "An energy harvesting system using the wind-induced vibration of a stay cable for powering a wireless sensor node," *Smart Materials and Structures*, 20, 075001

Kwon, S. (2010), "A T-shaped piezoelectric cantilever for fluid energy harvesting," *Applied Physics Letters*, 97(16), http://dx.doi.org/10.1063/1.3503609

Larsen, A. (1997), "Prediction of aeroelasstic stability of suspension bridges during erection," *Journal of Wind Engineering and Industrial Aerodynamics*, 72, 265-274.

Larsen, A. (1998), "Advanced in aeroelastic analyses of suspension and cable-stayed bridges," *Journal of Wind Engineering and Industrial Aerodynamics*, 74-76, 73-90.

Larsen, A. and Walther, J.H. (1998), "Discrete vortex simulation of flow around five generic bridge deck sections," *Journal of Wind Engineering and Industrial Aerodynamics*, 77&78, 591-602.

Li, S., Yuan, J. and Lipson Hod (2011), "Ambient wind energy harvesting using cross-flow fluttering," *Journal of Applied Physics*, 109, http://dx.doi.org/10.1063/1.3525045

Morgenthal, G. (2002), *Aerodynamic Analysis of Structures Using High-resolution Vortex Particle Methods*, PhD Dissertation, University of Cambridge, UK.

Morgenthal, G. (2000), *Fluid-Structure Interaction in Bluff-Body Aerodynamics and Long-Span Bridge Design: Phenomena and Methods*, Tech. Rep. CUED/D-STRUCT/TR.187, University of Cambridge, UK.

Morgenthal, M. (2007), "An Immersed Interface Method for the Vortex-in-Cell Algorithm," *Computers and Structurs*, 85, 712-726.

Roundy, S. and Wright, P.K. (2004), "A piezoelectric vibration based generator for wireless electronics," *Smart Materials and Structures*, 13, 1131-1142.

Scanlan, R.H. and Tomko, J.J. (1971), "Airfoil and bridge deck flutter derivatives," *Journal of Engineering Mechanics*, 97, 1717-1737

Sun, C., Shi, J., Bayerl, D.J. and Wang, X. (2011), "PVDF microbelts for harvesting energy from respiration," *Energy and Environmental Science*, 4, 4508-4512.